On the behaviour of a combined wind-wave energy conversion platform under energy-maximising control conditions

1st Maria Luisa Celesti
Marine Offshore Renewable Energy Lab.
Politecnico di Torino
Turin, Italy
marialuisa.celesti@studenti.polito.it

2nd Bruno Paduano
Marine Offshore Renewable Energy Lab.
Politecnico di Torino
Turin, Italy
bruno.paduano@polito.it

3rd Yerai Peña-Sanchez
Department of Mathematics
Euskal Herriko Unibertsitatea
Bilbao, Basque Country
yerai.pena@ehu.eus

4th Edoardo Pasta
Marine Offshore Renewable Energy Lab.
Politecnico di Torino
Turin, Italy
edoardo.pasta@polito.it

5th Nicolás Faedo
Marine Offshore Renewable Energy Lab.
Politecnico di Torino
Turin, Italy
nicolas.faedo@polito.it

6th John V. Ringwood
Centre for Ocean Energy Research
Maynooth University
Maynooth, Ireland
john.ringwood@mu.ie

***Abstract*—Climate changes are increasingly impacting human welfare and, together with population growth, are rising the energy demand. To mitigate their negative effects, the need to harvest energy from renewable sources, while reducing the dependency on fossil fuels, has become pressing. This has led to the pursuit of new concepts that can exploit natural resources efficiently. In this scenario, offshore wind-wave hybrid platforms have been recently promoted: sharing facilities, infrastructure, and grid connections, gives these systems the potential to increase energy production at a lower cost. However, an efficient realisation of these two combined technologies requires two potentially conflicting control objectives: On the one hand, for the wind turbine, a reduced motion of the platform is required, which essentially translates to enhanced stability of the structure, so that its behaviour resembles standard onshore wind technologies. On the other hand, to maximise the energy produced, wave energy converters (WECs) require optimal control technology which often leads to large amplitude motion, potentially conflicting with the stability required for the wind turbine. The aim of this study is to provide a better understanding of how the energy-maximising control problem for WEC systems interacts with both conversion systems, and to elucidate their corresponding synergies. A semi-submersible platform with an incorporated flap-type WEC is analysed from a closed-loop perspective, with the control system designed to maximise the energy produced by the WEC.**

***Index Terms*—Wave energy, Offshore wind, Combined wind-wave, Impedance-matching**

I. Introduction

Wind and wave sources have a high potential for providing clean and sustainable energy. While wave energy is still in an early stage of development, wind energy can count on mature technologies to exploit this resource. However, wave energy has a significant potential to contribute to the renewable energy mix [1]. In fact, the physical properties of waves, with higher energy density and predictable occurrence, make these a very powerful candidate energy resource [2]. As a matter of fact, a mix of wind and wave has the potential to provide a more stable, consistent, and efficient source of renewable energy [3]. Harnessing the power of both sources can greatly help in the pathway towards reducing the dependence on fossil fuels, and mitigating the environmental impact of their use.

As a consequence, the development and improvement of technologies to efficiently harness the potential of wind and wave sources are equally essential. Hybrid concepts, combining offshore wind turbines along with wave energy converters (WECs), are considered promising solutions to more sustainable energy systems [4]. As a matter of fact, being capable of sharing support structures, infrastructures, and grid connections, these combined systems have the great advantage of optimising the use of the ocean space, while reducing the relevant costs of installation, operation, and maintenance [5]. Overall, combining the two technologies in a synergetic fashion offers the possibility to enhance their performance. Large amplitude motions, to which floating offshore wind turbines are potentially subject to during operational sea states, can be counteracted by appropriate use of a WEC to minimise platform motion, as opposed to the standard use of passive damping systems, which simply dissipate the wave-induced energy [6]. In this way, wind-wave conversion platforms, being designed to harness both resources, can potentially increase the overall energy output of the system compared to traditional stand-alone wind or wave energy systems.

Though having a great potential to help in the pathway towards mitigation of emissions, wind-wave platforms still present a number of open challenges. In particular, their efficient realisation requires two potentially conflicting control objectives. In fact, a reduced platform movement is ideally required for the operation of the wind turbine, while large am-

979-8-3503-3226-1/23/$31.00 ©2023 IEEE

plitude motion is often the result of optimal control technology to reach energy-maximisation for WECs (see *e.g.* [7]). This study sets itself to provide deep insight, and hence a better understanding, of the key aspects and trade-offs underlying a synergistic operation of wind and wave energy concepts, through the design of energy-maximising control, based on the principle of *impedance-matching* [8], [9], in terms of *reactive* (proportional-integral - PI) and *passive* (proportional - P) controller structure, and corresponding detailed dynamical analysis.

The remainder of this paper is organised as follows. Section II briefly recalls the fundamentals of hydrodynamic modelling of floating structures. Section III provides a description of the case study presented within this paper, including definition of the wind-wave system, and associated energy-maximising control design procedure. Finally, Section IV illustrates the main numerical results obtained within this study, while Section V offers an overview of the conclusions.

II. Modelling fundamentals

Within this section, the modelling fundamentals for floating structures, in terms of linear potential flow theory, are briefly recalled. We begin by noting that WEC systems do not count yet with a 'standardised' device, *i.e.* there is no definitive concept available. This is mainly due to the fact that there are different ways in which wave energy can be absorbed and, depending on the location, water depth, and purpose for which they are used, different (more suitable) WEC concepts might be applicable [10], [11]. On the other hand, wind turbines, which are a much more mature technology, are already well-defined, with convergence to a single concept, *i.e.* the three-bladed turbine [12], [13]. Nonetheless, floating offshore wind turbines (FOWTs) can present different foundations, *e.g.* semi-submersible, spar-type, barge, and tension leg platform [14]. As such, the process of merging different wind turbine foundations and WECs with diverse working principles, gives origin to several hybrid wind-wave conversion platforms [15]. Within this study, and with the aim of deriving a set of generic conclusions and recommendations on the operation of hybrid wind-wave concepts, a representative case study is chosen, as described in detail within Section III.

The device hydrodynamics are described in terms of linear potential flow theory, hence describing the combined platform dynamics by means of linear equations [16]. Therefore, the equation of motion can be written in terms of a system of linear differential equations, *i.e.* the floating body dynamics can be described as

$$M\ddot{z}(t) = f_e(t) + f_r(t) + f_{re}(t) - u(t), \tag{1}$$

where z denotes the displacement vector associated with the structure (in all considered degrees-of-freedom (DoFs)), M is the generalised inertia-mass matrix of the floating system, f_e the wave excitation force/torque (*i.e.* the force/torque exerted on the structure by action of the incoming wave field), f_r the radiation force (dissipation action due to memory effects associated with the fluid response), f_{re} the hydrostatic restoring force, and u is the control input applied through the power take-off (PTO) system of the WEC device.

Under linear potential theory, the restoring force is given by $f_{re} = s_h z$, where s_h represents the so-called hydrostatic stiffness. The radiation force f_r is also modelled based on linear assumptions, using the well-known Cummins' equation [17], and can be numerically characterised using boundary element solvers.

Finally, the control input u is designed and synthesised based on the complex-conjugate impedance-matching [8] condition in which, to maximise converted energy, the PTO impedance is adjusted (via modification of the control 'load') to match the complex-conjugate of the mechanical impedance characterising the WEC DoF, as discussed explicitly within Section III. Note that the main objective of WEC control is to enable optimal energy capture from ocean waves via the associated PTO system. However, the energy available in ocean waves varies over time due to changes in wave height, wave period, and wave direction. Therefore, WECs must be able to adjust their motion in response to the changing wave conditions to capture as much energy as possible. In summary, adequate control technology is crucial to ensure maximum energy extraction from ocean waves, improving reliability and reducing the associated levelised cost of energy (LCOE) [18].

III. Case study and controller definition

Among the many existing wind-wave hybrid concepts (see the discussion provided in Section II), within this study, one of the most wide-spread is chosen as a representative case: the so-called *WindWaveFloat* system [19]. This combined concept, concentrating several devices on one platform, has the potential to offer both economic and operational advantages. In particular, the system, considered within this study, consists of a three-column semi-submersible platform with a standard horizontal-axis wind turbine (NREL 5 MW) at the top of a tower, sitting on the rear column, and a rectangular flap-type WEC mounted on the main beam. The devices taken as reference are the WindWaveFloat platform (as in [19]), and the *Oyster* WEC (see [20]).

The selected components (*i.e.* platform and WEC) are scaled with respect to their original size, as it can be appreciated in I. In particular, the flap dimensions are almost the same size as that characterising a full-scale Oyster system, while the semi-submersible platform is half the size of the WindWaveFloat reported in [19]. This is performed to assess the interaction of the WEC system with a smaller platform which, if operated correctly, can have substantial economical benefits for the overall system. We further note that the selected wind turbine is standard, and has been used as a reference in several wind-wave combined platforms [21]–[23]. Though considered within the calculation of the floating structure response, the dynamical analyses performed within this study are conducted considering the overall platform directly, *i.e.* using platform pitching motion as a proxy for turbine pitching movement. The main parameters, associated with the considered wind-wave platform, are summarised in Table I, while the mesh used for

computation of the corresponding hydrodynamic parameters is presented in Figure 1.

TABLE I
MAIN PARAMETERS OF THE WIND-WAVE STRUCTURE WITH RESPECT TO THE STILL WATER LEVEL.

Flap width	1.5 [m]
Flap length	15 [m]
Flap draft	6.5 [m]
Platform cylinder radius	5 [m]
Platform draft	15 [m]

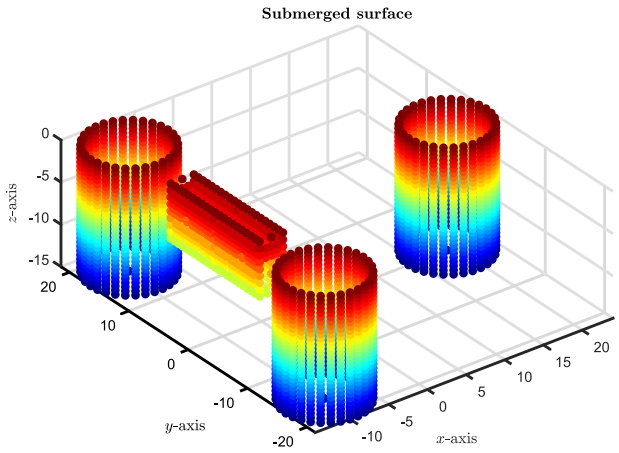

Fig. 1. Low order mesh used for computation of the hydrodynamic coefficients of the combined wind-wave platform using OrcaWave.

For the computation of the hydrodynamic coefficients associated with the system (*i.e.* the characterisation offered in equation (1)), the boundary element method (BEM) solver OrcaWave has been used [24]. The device considered within this study is identified in terms of 2 DoFs, *i.e.* pitch of both platform and WEC. Note that energy extraction for the WEC device effectively happens with the PTO system sitting on the pitch axis, and hence the system can be described in an input/output (I/O) form via direct application of the Laplace transform[1] to (1) as follows[2]

$$\begin{bmatrix} V_p \\ V_f \end{bmatrix} = \underbrace{\begin{bmatrix} G_{11} & G_{12} \\ G_{21} & G_{22} \end{bmatrix}}_{G} \begin{bmatrix} F_p \\ F_f - U \end{bmatrix}, \tag{2}$$

where $G : \mathbb{C} \to \mathbb{C}^{2\times 2}$, $s \mapsto G(s)$, is the transfer function map associated with the combined wind-wave system, which can be computed directly from the data obtained with the BEM solver, and where $\{v_p, v_f\}$ and $\{f_p, f_f\}$ denote pitch velocities and excitation torque components associated with platform and flap (WEC) system, respectively. Note that the map G can be decomposed in terms of its four entries, *i.e.* G_{11}, G_{12}, G_{21}, G_{22}, with $G_{12} = G_{21}$ due to the inherent symmetry of the hydrodynamic interactions between platform and WEC. In particular, $\{G_{11}, G_{12}\}$ define the I/O response for the platform, while the set $\{G_{21}, G_{22}\}$ characterises the pitch velocity of the WEC.

Following the discussion provided in Section II, we now proceed with the design of the control force u, acting on the flap system, in order to maximise the energy output of the WEC, by leveraging the principle of impedance-matching. In particular, exploiting the framework in [8], [9], we begin by noting that the WEC velocity can be written in compact form as

$$V_f = G_{22}[\tilde{F} - U], \tag{3}$$

where $\tilde{F}$ is the so-called *total* wave excitation force acting on the WEC controlled DoF, and it is given by

$$\tilde{F} = F_f + \frac{G_{21}}{G_{22}} F_p. \tag{4}$$

With the derivation of equation (3), the equivalent intrinsic impedance $I : \mathbb{R} \to \mathbb{C}$, $\omega \mapsto I(\omega)$, associated with the flap system, can be simply defined [8], [9] as

$$I(\omega) = \frac{1}{G_{22}(\jmath\omega)}. \tag{5}$$

Note that, with the definition of (4), the arguments used for the derivation of the impedance-matching optimal condition in [8], [9] can be applied straightforwardly. In particular, the optimal control condition can be written, in the frequency-domain, in terms of the complex-conjugate of (5), *i.e.*

$$U^{\text{opt}} = I_u V_f, \tag{6}$$

with the so-called control 'load' I_u defined as

$$I_u(\omega) = I^*(\omega) = \frac{1}{G^*_{22}(\jmath\omega)}. \tag{7}$$

Though effectively providing an energy-maximising control condition, as extensively discussed in [8], [9], the optimal control condition in (7) cannot be physically implemented, due to the very nature of the complex-conjugate operator. Nevertheless, a practical approximation of this condition can be achieved by means of causal and stable parametric controllers. As per the discussion provided in Section I, two well-known structures are commonly considered within the WEC control literature, *i.e.* the so-called passive (proportional - P) and reactive (proportional-integral - PI) controllers. In particular, using the impedance-matching conditions derived above, a reactive implementable controller in terms of a PI structure can be achieved as follows:

$$K_{PI}(s) = \theta_1 + \frac{\theta_2}{s}, \tag{8}$$

where θ_1 and θ_2 are designed to interpolate the optimal control impedance I_u in (7) at a specific input frequency ω_i.

The selection of the interpolation point, in the case of a sea-state that can be fully characterised in terms of the spectral density function with a certain peak period, T_p, can be chosen according to the corresponding peak frequency, $\omega_p = 2\pi/T_p$.

[1]Given a time-domain function f, its Laplace/Fourier transform is denoted as F, where the use of Laplace or Fourier is always clear from the context.

[2]From now on, the dependence on s or ω is dropped when clear from the context.

It is straightforward to show that the following parameter selection

$$\theta_1 = \Re(I_u(\omega_p)), \qquad \theta_2 = -\omega_p \Im(I_u(\omega_p)) \tag{9}$$

leads to the interpolation condition $K_{PI}(\omega_p) = I_u(\omega_p)$. Within Figure 2, it can be appreciated how the structure K_{PI} in (8) (dotted lines) interpolates I_u (solid line) at the corresponding pre-selected peak frequency. Naturally, a change of this peak input frequency generates a different corresponding optimal impedance value, and hence different PI parameters. In other words, there is an optimal PI control structure for each specific sea-state: θ_1 and θ_2 are effectively functions of the specific operating condition, as per equation (9).

Another important aspect to highlight, within Figure 2, is that in resonance condition (blue), *i.e.* when ω_i equals the natural frequency of the system, the optimal control K_{PI}, having zero phase in the Bode plot, is simply a constant value, and it hence becomes passive, *i.e.* proportional.

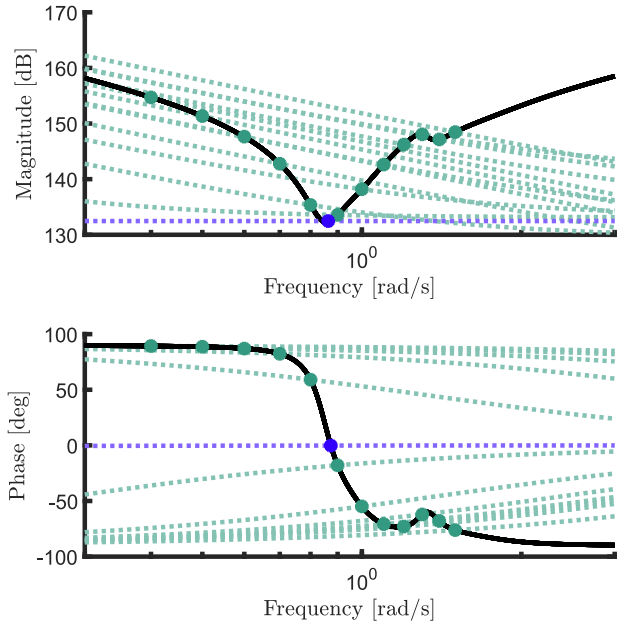

Fig. 2. Frequency response for the optimal control impedance (solid line), and each corresponding K_{PI} (dotted lines).

For the case of the passive control, *i.e.* proportional, the controller is defined in terms of a single parameter:

$$K_P(s) \equiv K_P = \theta_p, \tag{10}$$

where the damping value θ_p is given by

$$\theta_p = |I_u(\omega_i)|. \tag{11}$$

Note that reactive controllers are slightly more complex than their passive counterpart: a stiffness term is added in order to control not only the amplitude of the closed-loop response, but also its associated phase, being able to achieve optimal impedance-matching in a wide range of conditions, by a suitable change of the interpolation frequency. However, the choice between passive and reactive controllers depends on the specific requirements, application, and available (PTO) resources. In particular, in Section IV, the different impact that these two control parameterisations can have on the overall device dynamics, in terms of absorbed energy, is analysed in detail.

IV. Numerical results

This section presents a numerical appraisal of the application of the energy-maximising control structure described in Section III for the combined wind-wave platform, and the subsequent impact on system motion and overall response. In particular, for the results presented within this section, a set of irregular wave inputs is considered, based on a stochastic JONSWAP representation [25]. In particular, waves are generated with a fixed significant wave height of 1 [m], and peak wave periods in the set $\mathcal{W} = [0.8\omega_f,\ 1.2\omega_f]$, where ω_f denotes the resonance frequency (in pitch) associated with the WEC, highlighted with an arrow in Figure 3. Since a specific location in which the device could operate is not identified, to keep any conclusions as generic as possible, standard parameters are selected for the JONSWAP spectrum, *i.e.* a peak enhancement factor γ of 3.3.

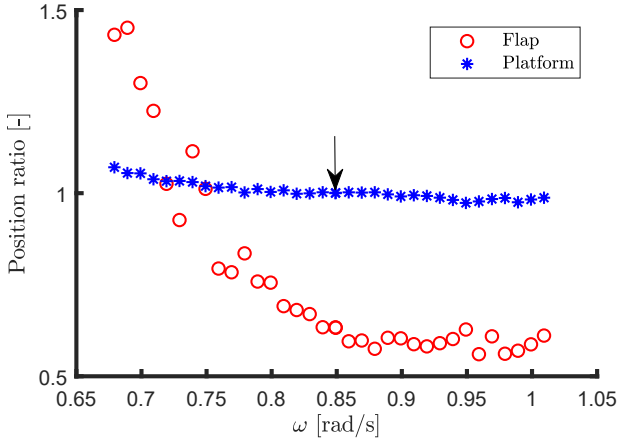

Fig. 3. Ratio of the root mean square value of flap and platform pitch position in PI controlled/uncontrolled WEC conditions.

Specifically, Figure 3 shows the ratio of the root mean square value of both flap and platform pitch position in PI controlled/uncontrolled WEC conditions, computed in steady-state, for a sufficiently large time window. Interestingly, considering the range of frequencies before resonance, a significantly larger amplitude motion can be seen for the flap and, at the same time, a relatively mild change in displacement of the platform, having an almost constant ratio for the full range of waves considered.

Another interesting aspect to evaluate is the order of magnitude of the control force to reach the energy-maximising objective. In Figure 4, the ratio of the control force and the root mean square value of flap and platform (excitation) torques are reported, considering as input the same set of irregular waves used in Figure 3. In addition, the ratio with respect to $\tilde{F}$, as defined in Equation (4), is also included.

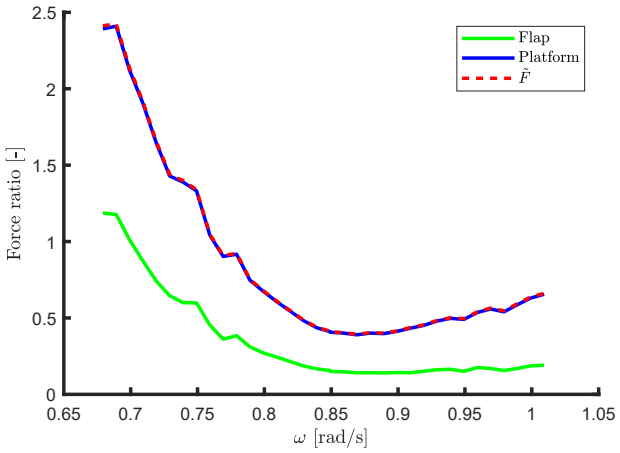

Fig. 4. Ratio of the root mean square value of flap and platform forces and the control force.

Note that, when the value of this ratio is greater than 1, the control action applied through the WEC is effectively larger than the torque experienced by the devices due to the incoming waves. Furthermore, In the range of frequencies where the significant input frequency ω_i (effectively used to synthesise the PI controller as in (9)) approaches the pitch resonance of the flap ω_f, the control force needed to reach energy-maximisation is effectively smaller. In fact, as can be appreciated from Figure 4, there is a consistent decrease in ratio, meaning that a combined wind-wave device with a WEC resonance frequency close to that characterising the incoming waves field requires a milder control action to reach the energy-maximisation objective.

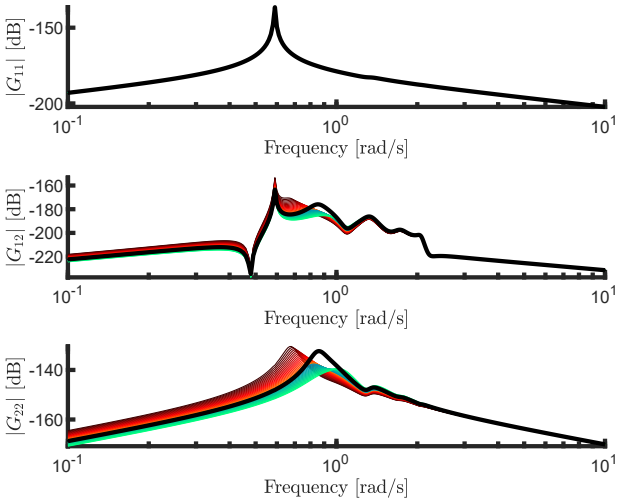

Fig. 5. Magnitude of the frequency response of the open-loop and closed-loop system: G_{11} (top), G_{12} (centre), G_{22} (bottom).

To further expand the results illustrated within Figures 3 and 4, a frequency-domain analysis of the overall input/output (torque/velocity) system is presented. Figure 5 illustrates (in black) the magnitude of the frequency response[3] associated with the (open-loop) map G in (2). In addition, Figure 5 presents the corresponding magnitude for the flap-controlled (*i.e.* closed-loop) system, when the wave input frequency ω_i, used for the interpolation of the impedance-matching condition with the corresponding PI structure (see equation (9)) is smaller (in red), and larger (in green), than the open-loop WEC resonance frequency ω_f. Note that, as the frequency ω_i decreases, the 'peak' that refers to the controlled WEC resonance moves accordingly (*i.e.* effective resonance with the wave peak frequency is achieved), becoming closer to the resonant behaviour of the platform. Furthermore, the magnitude associated with the interaction map between WEC and platform, *i.e.* G_{12}, has a consistently increasing trend, meaning that a stronger influence of the flap is present when the associated control system is designed to extract energy in waves close to the platform resonance.

[3]Only G_{12} is presented due to the hydrodynamic symmetry with G_{21}.

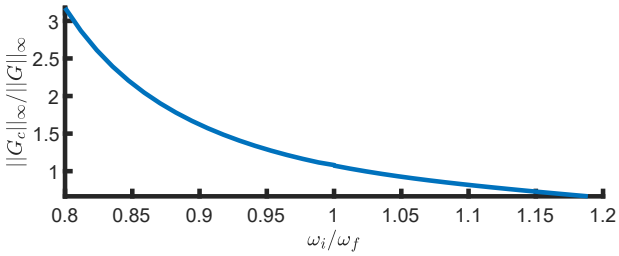

Fig. 6. Ratio of the $\mathscr{H}_\infty$-norm of the system in the controlled/uncontrolled conditions.

To expand the statement offered immediately above, Figure 6 presents a numerical appraisal of the interaction ratio between WEC and platform in terms of the associated $\mathscr{H}_\infty$-norm for G_{12} in controlled and uncontrolled conditions, as a function of the normalised input (interpolation) frequency ω_i/ω_f. It is straightforward to see that a lower frequency ω_i effectively increases the level of interaction between the two systems due to the controlled dynamics of the flap.

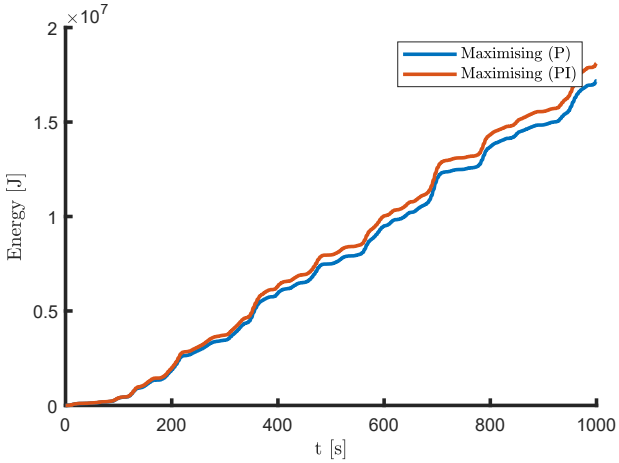

Fig. 7. Energy comparison between passive (P) and reactive (PI) control.

Finally, and to provide a comparison between the two control structures (*i.e.* PI and P) described within Section III,

Figure 7 presents the energy obtained with passive (P) and reactive (PI) controllers, for a particular irregular wave input case, with a wave peak frequency close to that characterising the resonance of the WEC (flap) system. It can be noticed that, for the full simulation, the value of energy obtained using a reactive controller is higher than the passive one, consistently with what expected from the synthesis procedure described in Section III. In fact, the PI controller, having two design parameters, can effectively interpolate the optimal energy-maximising condition, *i.e* achieve resonance between ovearll device motion and incident wave field, hence increasing the energy output.

V. Conclusion

This paper attempts at providing insight on the dynamics associated with a combined wind-wave platform under energy-maximising WEC control conditions. Overall, a clear interaction between WEC and platform, for a specific range of frequencies, is demonstrated when the device is under energy-maximising control conditions. In particular, the results indicate that the coupling between WEC and platform can change significantly when the former is controlled to maximise energy absorption from the incoming wave field. Depending on how close is the interpolation frequency ω_i to the platform resonance behaviour, this can be detrimental from the wind energy perspective, potentially leading to motion (pitching) values that can be prohibitive for a normal operation of the wind turbine. Nonetheless, the interaction between WEC and platform can be effectively beneficial for the overall energy absorption of the combined system in certain operational regimes, by extracting wave energy without a massive change in platform behaviour, hence exploiting the underlying synergies between both technologies.

References

[1] A. M. Cornett, "A global wave energy resource assessment," in *The Eighteenth international offshore and polar engineering conference*. OnePetro, 2008.

[2] O. Langhamer, K. Haikonen, and J. Sundberg, "Wave power—sustainable energy or environmentally costly? a review with special emphasis on linear wave energy converters," *Renewable and Sustainable Energy Reviews*, vol. 14, no. 4, pp. 1329–1335, 2010.

[3] F. Fusco, G. Nolan, and J. V. Ringwood, "Variability reduction through optimal combination of wind/wave resources–an irish case study," *Energy*, vol. 35, no. 1, pp. 314–325, 2010.

[4] K. L. McTiernan and K. T. Sharman, "Review of hybrid offshore wind and wave energy systems," in *Journal of Physics: Conference Series*, vol. 1452, no. 1. IOP Publishing, 2020, p. 012016.

[5] D. M. Skene, N. Sergiienko, B. Ding, and B. Cazzolato, "The prospect of combining a point absorber wave energy converter with a floating offshore wind turbine," *Energies*, vol. 14, no. 21, p. 7385, 2021.

[6] M. Borg, M. Collu, and F. P. Brennan, "Use of a wave energy converter as a motion suppression device for floating wind turbines," *Energy Procedia*, vol. 35, pp. 223–233, 2013.

[7] C. Windt, N. Faedo, M. Penalba, F. Dias, and J. V. Ringwood, "Reactive control of wave energy devices–the modelling paradox," *Applied Ocean Research*, vol. 109, p. 102574, 2021.

[8] N. Faedo, F. Carapellese, E. Pasta, and G. Mattiazzo, "On the principle of impedance-matching for underactuated wave energy harvesting systems," *Applied Ocean Research*, vol. 118, p. 102958, 2022.

[9] N. Faedo, E. Pasta, F. Carapellese, V. Orlando, D. Pizzirusso, D. Basile, and S. A. Sirigu, "Energy-maximising experimental control synthesis via impedance-matching for a multi degree-of-freedom wave energy converter," *IFAC-PapersOnLine*, vol. 55, no. 31, pp. 345–350, 2022.

[10] R. Pelc and R. M. Fujita, "Renewable energy from the ocean," *Marine Policy*, vol. 26, no. 6, pp. 471–479, 2002.

[11] A. F. d. O. Falcão, "Wave energy utilization: A review of the technologies," *Renewable and sustainable energy reviews*, vol. 14, no. 3, pp. 899–918, 2010.

[12] P. J. Schubel and R. J. Crossley, "Wind turbine blade design," *Energies*, vol. 5, pp. 3425–3449, 2012.

[13] *Basic Concepts of Wind Energy Converters*. Berlin, Heidelberg: Springer Berlin Heidelberg, 2006, pp. 67–80.

[14] X. Dong, Y. Li, D. Li, F. Cao, X. Jiang, and H. Shi, "A state-of-the-art review of the hybrid wind-wave energy converter," *Progress in Energy*, vol. 4, p. 042004, 2022.

[15] J. Hu, B. Zhou, C. Vogel, P. Liu, R. Willden, K. Sun, J. Zang, J. Geng, P. Jin, L. Cui, B. Jiang, and M. Collu, "Optimal design and performance analysis of a hybrid system combing a floating wind platform and wave energy converters," *Applied Energy*, vol. 269, 2020.

[16] M. Alves, "Frequency-domain models," in *Numerical Modelling of Wave Energy Converters*. Elsevier, 2016, pp. 11–30.

[17] W. Cummins, "The impulse response function and ship motions," David Taylor Model Basin Washington DC, Tech. Rep., 1962.

[18] J. V. Ringwood, G. Bacelli, and F. Fusco, "Energy-maximizing control of wave-energy converters: The development of control system technology to optimize their operation," *IEEE control systems magazine*, vol. 34, no. 5, pp. 30–55, 2014.

[19] A. Weinstein, D. Roddier, and K. Banister, "Windwavefloat (wwf): Final scientific report," Principle Power Inc., United States, Tech. Rep., 2012.

[20] T. Whittaker, D. Collier, M. Folley, M. Osterried, A. Henry, and M. Crowley, "The development of oyster—a shallow water surging wave energy converter," in *Proceedings of the 7th European wave and tidal energy conference*, 2007, pp. 11–14.

[21] N. Ren, Z. Ma, B. Shan, D. Ning, and J. Ou, "Experimental and numerical study of dynamic responses of a new combined tlp type floating wind turbine and a wave energy converter under operational conditions," *Renewable Energy*, vol. 151, pp. 966–974, 2020.

[22] N. Ren, Z. Ma, T. Fan, G. Zhai, and J. Ou, "Experimental and numerical study of hydrodynamic responses of a new combined monopile wind turbine and a heave-type wave energy converter under typical operational conditions," *Ocean engineering*, vol. 159, pp. 1–8, 2018.

[23] S. Jovašević, M. R. S. Mohammadi, C. Rebelo, M. Pavlović, and M. Veljković, "New lattice-tubular tower for onshore wec–part 1: Structural optimization," *Procedia engineering*, vol. 199, pp. 3236–3241, 2017.

[24] Orcina, "OrcaFlex - Documentation, 10.1b Edition," Tech. Rep., 2020. [Online]. Available: https://www.orcina.com/SoftwareProducts/OrcaFlex/Documentation/

[25] D. E. Hasselmann, M. Dunckel, and J. Ewing, "Directional wave spectra observed during JONSWAP 1973," *Journal of physical oceanography*, vol. 10, no. 8, pp. 1264–1280, 1980.